

**Bottle-brush polymers as an intermediate between star and cylindrical polymers**

N. A. Denesyuk\*

*Department of Chemistry, University of Cambridge, Lensfield Road, Cambridge CB2 1EW, United Kingdom*  
(Received 25 February 2003; revised manuscript received 23 June 2003; published 18 September 2003)

We present a theoretical study of a single bottle-brush molecule, which consists of multiarmed polymer stars grafted densely onto a stiff backbone. Mean-field approximation and a variational approach are used to calculate the dominant trajectories of the grafted chains, the shape of the molecule, and the segment density distribution around the backbone. All these properties are calculated for an arbitrary relationship between the size of the backbone and that of a grafted star. Hence cylindrical comb copolymer brushes and spherically symmetric polymer stars are considered as the limiting cases of the present problem.

DOI: 10.1103/PhysRevE.68.031803

PACS number(s): 61.41.+e, 81.05.Lg

**I. INTRODUCTION**

In this paper, we carry out a theoretical investigation of cylindrical comb copolymer brushes or bottle-brush molecules [1–9]. We assume that such molecules are composed of multi-armed polymer stars, grafted densely onto a rigid or flexible backbone. In our previous work [9], we considered the particular case of a flexible backbone and side chains of the same chemical composition. We showed that, in the presence of excluded volume interactions, a bottle-brush molecule can be found in one of the three conformational states, depending on the backbone's molecular weight. Here we briefly summarize the results obtained in Ref. [9].

First, let us consider a backbone of very low molecular weight, so that its length  $L$  is much shorter than the size of a grafted star. In this case, all the side chains in a bottle-brush molecule are virtually grafted onto the same point, and the molecule appears to be a single polymer star. The number of arms in such a star is given by the total number of the grafted chains, and these arms are swollen uniformly in all directions. Thus, for  $L \rightarrow 0$  the bottle-brush molecule is found in a spherically symmetric conformation. As the backbone length  $L$  grows but remains smaller than a certain crossover value  $L_c$ , the swelling of the side chains increases and eventually reaches a plateau at  $L \sim L_c$ . At the same time, in the presence of excluded volume interactions, the grafted chains try to avoid strong overlapping. This leads to a large increase in the stiffness of the backbone, so that its linear size  $L$  grows proportionally to the molecular weight. Consequently, for  $L > L_c$  the bottle-brush molecule acquires the shape of a long stiff cylinder, whose diameter is roughly given by the maximum size of the grafted chains. The critical backbone size  $L_c$  marks a crossover between spherical and cylindrical symmetries of a bottle-brush molecule. When the size of the backbone is very large, i.e.,  $L \gg L_c$ , the grafted chains can no longer restrict the backbone's folding and it adopts a spherically symmetric coil-like conformation.

In this paper, we present a quantitative study of the conformational crossover which occurs at the backbone sizes  $L \sim L_c$ . We assume that the backbone's molecular weight is not particularly high, and so the backbone itself can be mod-

eled as a (infinitely thin) stiff rod. On the other hand, we do not make any assumptions regarding the relationship between  $L$  and the linear size  $R_g$  of a grafted chain. In fact,  $L_c \sim R_g$ , and it is the ratio  $L/R_g$  which governs the crossover between the spherical ( $L/R_g \ll 1$ ) and cylindrical ( $L/R_g \gg 1$ ) conformations of a bottle-brush molecule. The polymer brushes of different symmetries are clearly described by different scaling laws, and it is interesting to study how these laws transform into each other as the parameter  $L/R_g$  changes. Herein, in order to study the transformation of the scaling laws, we consider a single bottle-brush molecule with the ratio  $L/R_g \ll 1$ . If we probe such a molecule very near its backbone, the influence of the backbone ends can be neglected and the molecule appears to be infinitely long. This implies that, in the close vicinity of the backbone, a bottle-brush molecule is described by the scaling relationships which are characteristic of cylindrical symmetry. However, at large distances from the backbone, the backbone's linear size  $L$  appears to be negligibly small and we should find the scaling relationships of a spherically symmetric polymer star.

Our analysis is largely based on using the variational approach, which was suggested in Ref. [4] to calculate the properties of the planar, spherical, and infinitely long cylindrical brushes. We generalize this approach to the case when the backbone size  $L$  is taken to be arbitrary. In the following sections, we give a detailed description of the examined bottle-brush molecule and calculate its properties such as the segment density distribution around the backbone, the dominant trajectories of the grafted chains, and the molecule's shape.

**II. DESCRIPTION OF THE MODEL AND THE FREE ENERGY FUNCTIONAL**

In this work we consider a bottle-brush molecule which consists of  $M$  stars, each containing  $f$  flexible chains of length  $N$ , grafted regularly onto a stiff backbone of length  $L$  (see Fig. 1 in Ref. [9]). We assume that the stars are grafted very densely, so that the interstar spacing  $d = L/(M-1)$  is much smaller than the size of the backbone  $L$ . The condition  $d \ll L$  implies high segment densities inside a polymer brush, which allows us to treat the problem within a mean-field approximation.

It is convenient to introduce the cylindrical coordinate

\*Electronic address: nad28@cam.ac.uk

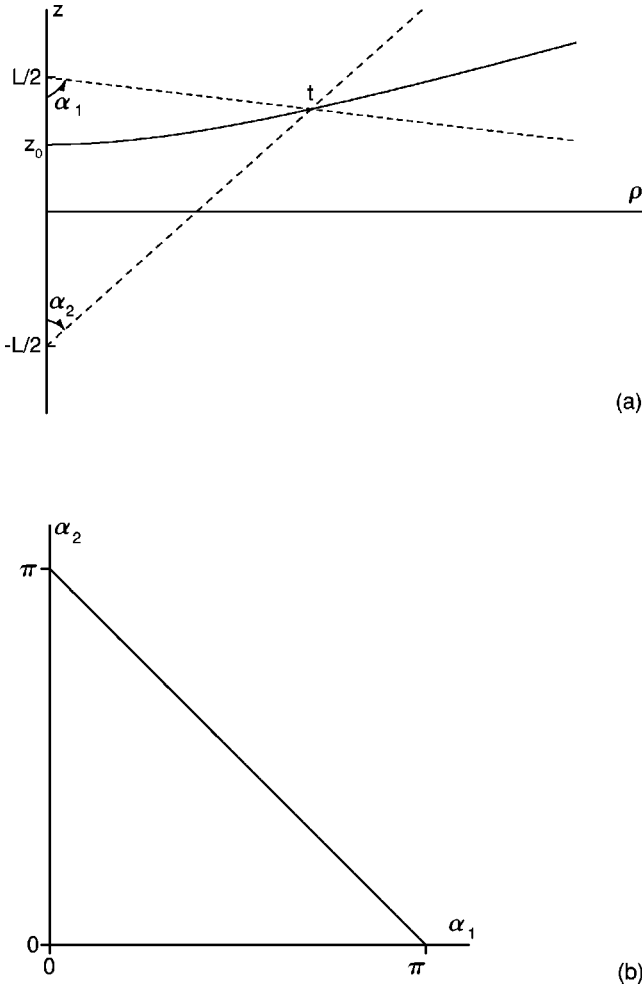


FIG. 1. Illustration of the cylindrical  $\{\rho, z\}$  and angle  $\{\alpha_1, \alpha_2\}$  coordinate systems, introduced in this paper. Note that the infinite half plane  $\{\rho > 0, z\}$  is transformed into the finite triangle  $\alpha_1 + \alpha_2 \leq \pi$ , shown in (b). The side  $\alpha_2 = 0$  ( $\alpha_1 = 0$ ) of this triangle represents the immediate vicinity of the upper (lower) end of the backbone, while the diagonal  $\alpha_1 + \alpha_2 = \pi$  corresponds to infinity in the half plane  $\{\rho > 0, z\}$ .

system  $\{\rho, z, \phi\}$ , where axis  $z$  is directed along the backbone [see Fig. 1(a)]. Due to symmetry, we do not need to consider the angle coordinate  $\phi$  and the problem becomes two dimensional. In this context, the variational approach amounts to writing down the molecule's free energy as a functional of two independent functions of two variables and minimizing it with respect to these functions. A possible choice for the independent functions is the dominant trajectories of grafted chains  $\{\rho = f_1(z_0, t), z = f_2(z_0, t)\}$ , where  $z_0$  and  $t$  stand, respectively, for the grafting point and the segment number of a given chain [Fig. 1(a)]. Alternatively, we can work with the space fields  $z_0 = f_3(\rho, z)$  and  $t = f_4(\rho, z)$ , which are defined as the functions inverse to  $f_1(z_0, t)$  and  $f_2(z_0, t)$ . In the following analysis, we will require all four functions.

The molecule's elastic free energy is expressed straightforwardly in terms of the chains' dominant trajectories,

$$F^{el} = \frac{3}{2a^2} \frac{f}{d} \int_{-L/2}^{L/2} dz_0 \int_0^N dt \left[ \left( \frac{\partial f_1}{\partial t} \right)^2 + \left( \frac{\partial f_2}{\partial t} \right)^2 \right], \quad (1)$$

where  $a$  denotes the segment size. Since  $d/L \ll 1$ , in Eq. (1) we substituted the summation over all side chains by the integral over  $z_0$ . Within a mean-field approximation, the interaction part of the free energy reads

$$F^{int} = \frac{v_e}{2} \int dz \int d\rho n^2(\rho, z) 2\pi\rho, \quad (2)$$

where  $v_e$  is the excluded volume parameter and  $n(\rho, z)$  stands for the segment density distribution around the backbone. We can calculate this distribution by choosing an elementary volume inside the polymer brush and counting the number of segments inside it. For simplicity, we assume that all the free ends are excluded from the brush's interior, which represents a natural extension of the Alexander-de Gennes approximation [10] used for a planar geometry. The resulting expression for  $n(\rho, z)$  is found to be proportional to the Jacobian

$$D(\rho, z) = \frac{\partial f_3}{\partial z} \frac{\partial f_4}{\partial \rho} - \frac{\partial f_3}{\partial \rho} \frac{\partial f_4}{\partial z}, \quad (3)$$

namely,

$$n(\rho, z) = \frac{f}{d} \frac{D(\rho, z)}{2\pi\rho}. \quad (4)$$

Equation (4) can also be expressed in terms of the variables  $z_0$  and  $t$ ,

$$n(z_0, t) = \frac{f}{d} \frac{1}{2\pi f_1(z_0, t) D_{-1}(z_0, t)}, \quad (5)$$

where

$$D_{-1}(z_0, t) = \frac{\partial f_1}{\partial t} \frac{\partial f_2}{\partial z_0} - \frac{\partial f_1}{\partial z_0} \frac{\partial f_2}{\partial t}. \quad (6)$$

Clearly, the Jacobian  $D_{-1}(z_0, t)$  is reciprocal to  $D(\rho, z)$ , i.e.,

$$DD_{-1} = 1. \quad (7)$$

Combining Eqs. (1)–(6) provides us with an expression for the total free energy as a functional of  $f_1$  and  $f_2$ ,

$$F[f_1, f_2] = \int_{-L/2}^{L/2} dz_0 \int_0^N dt \left\{ \frac{3}{2a^2} \frac{f}{d} \left[ \left( \frac{\partial f_1}{\partial t} \right)^2 + \left( \frac{\partial f_2}{\partial t} \right)^2 \right] + \frac{v_e}{2} \left( \frac{f}{d} \right)^2 \frac{1}{2\pi f_1 D_{-1}} \right\}. \quad (8)$$

### III. THE EULER-LAGRANGE EQUATIONS FOR THE TRAJECTORIES OF POLYMER CHAINS

#### A. Derivation of the Euler-Lagrange equations

Minimizing the free energy functional of Eq. (8) with respect to functions  $f_1$  and  $f_2$ , we obtain a system of two partial differential equations which determine the dominant trajectories of grafted chains,

$$\frac{\partial^2 f_1}{\partial t^2} + \frac{1}{D_{-1} f_1^2} + \frac{1}{D_{-1}^3 f_1} \left( \frac{\partial D_{-1}}{\partial t} \frac{\partial f_2}{\partial z_0} - \frac{\partial D_{-1}}{\partial z_0} \frac{\partial f_2}{\partial t} \right) = 0,$$

$$\frac{\partial^2 f_2}{\partial t^2} - \frac{1}{D_{-1}^3 f_1} \left( \frac{\partial D_{-1}}{\partial t} \frac{\partial f_1}{\partial z_0} - \frac{\partial D_{-1}}{\partial z_0} \frac{\partial f_1}{\partial t} \right) = 0. \quad (9)$$

When deriving these equations, we have made the following changes of variables:

$$f_1 \rightarrow f_1 l, \quad f_2 \rightarrow f_2 l, \quad \rho \rightarrow \rho l, \quad z \rightarrow z l, \quad n \rightarrow n l^{-3}, \quad (10)$$

where the length scale  $l$  is given by

$$l = \left( \frac{1}{6\pi} v_e a^2 \frac{f}{d} \right)^{1/4}. \quad (11)$$

Substituting Eq. (10) into Eqs. (3)–(6) yields the following expressions for the dimensionless density of polymer segments:

$$n = \frac{D}{\rho} = \frac{1}{f_1 D_{-1}}. \quad (12)$$

The physical meaning of Eqs. (9) becomes transparent if we rewrite these equations using the relationships

$$\frac{\partial f_1}{\partial t} = D_{-1} \frac{\partial f_3}{\partial z}, \quad \frac{\partial f_1}{\partial z_0} = -D_{-1} \frac{\partial f_4}{\partial z},$$

$$\frac{\partial f_2}{\partial t} = -D_{-1} \frac{\partial f_3}{\partial \rho}, \quad \frac{\partial f_2}{\partial z_0} = D_{-1} \frac{\partial f_4}{\partial \rho}, \quad (13)$$

and the general rules of partial differentiation. We find

$$\frac{\partial^2 f_1}{\partial t^2} - \frac{\partial}{\partial \rho} \left( \frac{1}{f_1 D_{-1}} \right) = 0,$$

$$\frac{\partial^2 f_2}{\partial t^2} - \frac{\partial}{\partial z} \left( \frac{1}{f_1 D_{-1}} \right) = 0, \quad (14)$$

or, in view of Eq. (12),

$$\frac{\partial^2 f_1}{\partial t^2} - \frac{\partial}{\partial \rho} n(\rho, z) = 0,$$

$$\frac{\partial^2 f_2}{\partial t^2} - \frac{\partial}{\partial z} n(\rho, z) = 0. \quad (15)$$

Thus, Eqs. (9) are equivalent to the Euler-Lagrange equations describing the motion of a classical particle in the external field  $\phi^{ext}(\rho, z) \equiv -n(\rho, z)$ . However, in the polymer case,  $n(\rho, z)$  corresponds to the self-consistent (and not to the external) field, i.e., the field which is itself determined by the trajectories of the grafted chains.

A simple and useful relationship for the segment density distribution  $n(\rho, z)$  can be obtained by substituting Eqs. (15) into the following very general law of partial differentiation:

$$\frac{\partial}{\partial t} n(z_0, t) = \frac{\partial f_1}{\partial t} \frac{\partial}{\partial \rho} n(\rho, z) + \frac{\partial f_2}{\partial t} \frac{\partial}{\partial z} n(\rho, z). \quad (16)$$

We obtain

$$\frac{\partial}{\partial t} \left[ \frac{1}{2} \left( \frac{\partial f_1}{\partial t} \right)^2 + \frac{1}{2} \left( \frac{\partial f_2}{\partial t} \right)^2 - n(z_0, t) \right] = 0, \quad (17)$$

so that the combination in square brackets remains constant along the chain trajectory. Note that, within the particle formulation of the problem, Eq. (17) corresponds to the energy conservation law. We assume that the stretching of chains is zero when the segment density  $n$  vanishes, which yields

$$n = \frac{1}{2} \left[ \left( \frac{\partial f_1}{\partial t} \right)^2 + \left( \frac{\partial f_2}{\partial t} \right)^2 \right]. \quad (18)$$

Equations (15) and (18), the boundary conditions

$$f_1(z_0, 0) = 0, \quad f_2(z_0, 0) = z_0, \quad (19)$$

as well as some symmetry restrictions determine uniquely the dominant trajectories of the grafted chains.

### B. Example: Solution of the Euler-Lagrange equations in the case of infinitely long cylindrical brush

For an infinitely long cylindrical brush, the problem becomes one dimensional and we can write

$$f_1(z_0, t) = f_1(t), \quad f_2(z_0, t) = z_0. \quad (20)$$

Combining Eqs. (12), (18), and (20) results in the nonlinear differential equation for the function  $f_1(t)$ ,

$$\left( f_1 \frac{df_1}{dt} \right)^{-1} = \frac{1}{2} \left( \frac{df_1}{dt} \right)^2, \quad (21)$$

whose solution is uniquely defined and reads

$$f_1(t) = \frac{2}{3} 2^{3/4} 3^{1/4} t^{3/4}. \quad (22)$$

Furthermore, we find for the segment density distribution,

$$n = \left( f_1 \frac{df_1}{dt} \right)^{-1} = \frac{\sqrt{6}}{4} t^{-1/2} = \frac{1}{2} 2^{2/3} \rho^{-2/3}. \quad (23)$$

This simple example shows that, within the present approach, the trajectories of all grafted chains, as well as the segment density distribution, are independent of the chain length  $N$ . However, we need to know  $N$  in order to specify the width  $\rho^*$  of a polymer brush and the total segment density  $n^*$  at its surface. From Eqs. (22) and (23), we get

$$\rho^* = \frac{2}{3} 2^{3/4} 3^{1/4} N^{3/4}, \quad (24)$$

$$n^* = \frac{\sqrt{6}}{4} N^{-1/2}. \quad (25)$$

We stress that the Alexander–de Gennes approximation yields the nonzero value  $n^*$  of the segment density at the surface of a polymer brush. Moreover, according to Eq. (18), the same holds for the stretching of chains at their free ends. This is, clearly, an artifact of the present approach. We believe, however, that if the degree of polymerization  $N$  of the grafted chains is high, there is an extensive region in the brush’s interior where Eqs. (24) and (25) are valid. In other words, we assume that the analytical prefactors that might appear in the above equations in order to satisfy the condition of continuously vanishing segment density will remain localized at the surface. The great advantage of such an approach is that it allows us to describe the polymer brushes of all sizes with only one set of equations and boundary conditions.

#### IV. OTHER REPRESENTATIONS OF THE EULER-LAGRANGE EQUATIONS

##### A. Cylindrical coordinates $\rho$ and $z$

For the purpose of solving the equations of motion, derived in the preceding section, it seems more convenient to work with the functions  $f_3(\rho, z)$  and  $f_4(\rho, z)$ . In this case, we have in place of Eqs. (15) and (18)

$$\begin{aligned} \frac{\partial}{\partial z} \left( \frac{x_1}{n} \right) + \frac{\partial}{\partial \rho} \left( \frac{x_2}{n} \right) &= 0, \\ \frac{\partial x_2}{\partial z} - \frac{\partial x_1}{\partial \rho} - \frac{x_1}{\rho} &= 0, \\ n^3 &= \frac{1}{2} (x_1^2 + x_2^2), \end{aligned} \quad (26)$$

where new functions  $x_1(\rho, z)$  and  $x_2(\rho, z)$  have been introduced,

$$x_1(\rho, z) = \frac{1}{\rho} \frac{\partial f_3}{\partial z}, \quad x_2(\rho, z) = \frac{1}{\rho} \frac{\partial f_3}{\partial \rho}. \quad (27)$$

The first and the third of Eqs. (26) are derived in Appendix A, whereas the second equation points to the fact that functions  $x_1$  and  $x_2$  are not independent [cf. Eq. (27)]. The boundary condition to Eqs. (26) follows straightforwardly from the definition of  $f_3$  [recall  $f_3(\rho, z) \equiv z_0$ ] and reads

$$x_1(\rho \rightarrow 0, z) = \frac{\Theta(L/2 - |z|)}{\rho}, \quad (28)$$

where  $\Theta(\zeta)$  is the Heaviside step function, defined as zero for  $\zeta < 0$ , 1 for  $\zeta > 0$ , and not defined at  $\zeta = 0$ . Once Eqs. (26) have been solved and  $f_3$  is known,  $f_4$  is found as a solution to the linear partial differential equation [see Eq. (12)],

$$D(\rho, z) = \rho n(\rho, z), \quad (29)$$

where  $D(\rho, z)$  is given by Eq. (3). Together,  $f_3$  and  $f_4$  determine implicitly the dominant trajectories of side chains. In

addition, we note that, as already shown for the case of an infinitely long cylindrical brush, the segment density distribution  $n$  is found to be independent of  $f_4$ , i.e., of the chain length  $N$ . (The discussion of this matter is presented in Sec. III B.)

##### B. Angle coordinates $\alpha_1$ and $\alpha_2$

Equations (26) represent a system of nontrivial partial differential equations which can be solved only numerically. In order to simplify the numerical calculations, we introduce the angle coordinates  $\alpha_1$  and  $\alpha_2$  [see Fig. 1(a)],

$$\tan \alpha_1 = \frac{\rho}{L/2 - z}, \quad \tan \alpha_2 = \frac{\rho}{L/2 + z}, \quad (30)$$

so that we can perform all integrations within the finite triangle  $\alpha_1 + \alpha_2 \leq \pi$  [Fig. 1(b)]. Furthermore, defining the new functions  $\Phi(\alpha_1, \alpha_2)$ ,  $R(\alpha_1, \alpha_2)$  and  $g(\alpha_1, \alpha_2)$ , such that

$$\begin{aligned} \frac{\partial f_3}{\partial z} &= R \cos \Phi, \quad \frac{\partial f_3}{\partial \rho} = R \sin \Phi, \\ f_4(\rho, z) &= \frac{1}{2^{1/3}} \rho^{4/3} g(\alpha_1, \alpha_2), \end{aligned} \quad (31)$$

enables us to derive the universal Euler-Lagrange equations which are independent of any length scales. Substituting Eqs. (30) and (31) into Eqs. (26), we find

$$\begin{aligned} \sin \alpha_1 \frac{\partial \ln R}{\partial \alpha_1} \sin(\Phi + \alpha_1) + \sin \alpha_2 \frac{\partial \ln R}{\partial \alpha_2} \sin(\Phi - \alpha_2) \\ + 3 \sin \alpha_1 \frac{\partial \Phi}{\partial \alpha_1} \cos(\Phi + \alpha_1) + 3 \sin \alpha_2 \frac{\partial \Phi}{\partial \alpha_2} \cos(\Phi - \alpha_2) \\ - \sin \Phi = 0, \\ \sin \alpha_1 \frac{\partial \ln R}{\partial \alpha_1} \cos(\Phi + \alpha_1) + \sin \alpha_2 \frac{\partial \ln R}{\partial \alpha_2} \cos(\Phi - \alpha_2) \\ - \sin \alpha_1 \frac{\partial \Phi}{\partial \alpha_1} \sin(\Phi + \alpha_1) - \sin \alpha_2 \frac{\partial \Phi}{\partial \alpha_2} \sin(\Phi - \alpha_2) = 0, \\ n^3 = \frac{1}{2\rho^2} R^2. \end{aligned} \quad (32)$$

Equations (32) include two partial differential equations (PDEs) that must be solved simultaneously to yield  $\Phi$  and  $\bar{R} = \ln R$ . Note that both PDEs are linear with respect to  $\bar{R}$ , which significantly simplifies their solution. Besides, we obtain from Eq. (29),

$$\begin{aligned} \frac{4}{3} g \cos \Phi + \sin \alpha_1 \frac{\partial g}{\partial \alpha_1} \cos(\Phi + \alpha_1) + \sin \alpha_2 \frac{\partial g}{\partial \alpha_2} \cos(\Phi - \alpha_2) \\ - R^{-1/3} = 0. \end{aligned} \quad (33)$$

The corresponding boundary conditions to Eqs. (32) and (33) read

$$\Phi(0,0)=0, \quad \bar{R}(0,0)=0, \quad g(0,0)=\frac{3}{4}. \quad (34)$$

### V. LINEARIZED EQUATIONS: SOLUTION AND DISCUSSION OF THE RESULTS

Equations (26) can be noticeably simplified if we suppose that the dominant trajectories of chains are everywhere perpendicular to a surface of constant density  $n(\rho, z) = n_0$ . Analytically, this condition can be expressed in the form

$$\frac{\partial n}{\partial \rho} \frac{\partial f_3}{\partial \rho} + \frac{\partial n}{\partial z} \frac{\partial f_3}{\partial z} = 0. \quad (35)$$

Substituting Eq. (35) into the first of Eqs. (26), as well as taking up the second of these equations, we arrive at the system of two linear partial differential equations with respect to functions  $x_1(\rho, z)$  and  $x_2(\rho, z)$ ,

$$\begin{aligned} \frac{\partial x_1}{\partial z} + \frac{\partial x_2}{\partial \rho} &= 0, \\ \frac{\partial x_2}{\partial z} - \frac{\partial x_1}{\partial \rho} &= \frac{x_1}{\rho}. \end{aligned} \quad (36)$$

The solution to Eqs. (36) under the boundary condition of Eq. (28) reads

$$\begin{aligned} x_1(\rho, z) &= \frac{1}{2\rho} \left[ \frac{z+1}{\sqrt{\rho^2 + (z+1)^2}} + \frac{1-z}{\sqrt{\rho^2 + (1-z)^2}} \right], \\ x_2(\rho, z) &= \frac{1}{2} \left[ \frac{1}{\sqrt{\rho^2 + (z+1)^2}} - \frac{1}{\sqrt{\rho^2 + (1-z)^2}} \right], \end{aligned} \quad (37)$$

and

$$f_3(\rho, z) = \frac{1}{2} \left[ \sqrt{\rho^2 + (z+1)^2} - \sqrt{\rho^2 + (1-z)^2} \right]. \quad (38)$$

Note that in the above equations, and everywhere in the further analysis, we set the half-length of the backbone equal to one, i.e.,  $L/2 \equiv 1$ . Equation (38) determines the dominant trajectories of grafted chains via the relationship  $f_3(\rho, z) = z_0$ , and we have

$$z(\rho, z_0) = z_0 \sqrt{1 + \frac{\rho^2}{1 - z_0^2}}. \quad (39)$$

As shown in Fig. 2, the trajectories of all but the central chains (i.e., grafted at  $z_0 = 0$ ) are curved outwards from the center of the molecule, this curvature being stronger for those chains that are grafted closer to the ends of the backbone. Due to the bending of chains, the segment density inside a polymer brush is lowered, so is the interaction part of the free energy. Figure 3 shows the three-dimensional graph of the segment density distribution  $n(\rho, z)$  as it is given by the last of Eqs. (26). We note that the segment density diverges in the immediate vicinity of the backbone.

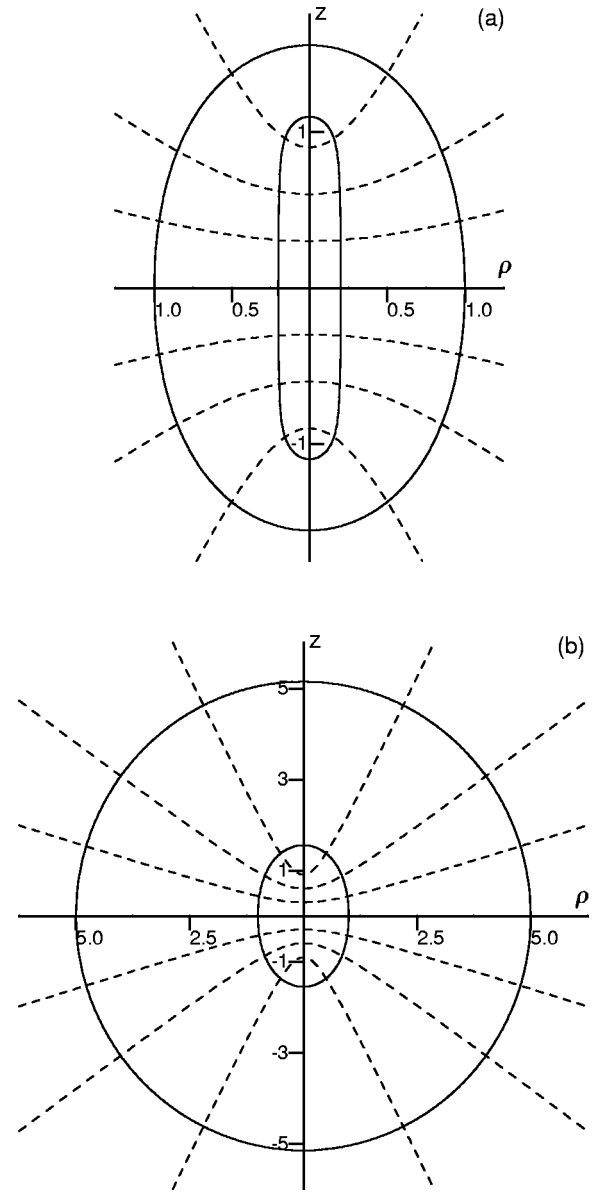


FIG. 2. The dominant trajectories of chains with grafting points  $z_0 = 0.3, 0.6,$  and  $0.9$  (dashed lines), and surfaces of constant density (solid lines), as obtained from the linearized Euler-Lagrange equations. The surfaces of constant density are chosen so as to give the following maximum values of coordinate  $\rho$ : (a)  $\rho_{max} = 0.2$  and 1, (b)  $\rho_{max} = 1$  and 5.

Along the line of a central chain, that is the line  $z = 0$ , the segment density distribution  $n(\rho, z)$  has the form

$$n(\rho) = \frac{1}{[2\rho^2(1 + \rho^2)]^{1/3}}. \quad (40)$$

Equation (40) reveals the following power law asymptotics:

$$n(\rho) \sim \begin{cases} \rho^{-2/3}, & \rho \ll 1 \\ \rho^{-4/3}, & \rho \gg 1, \end{cases} \quad (41)$$

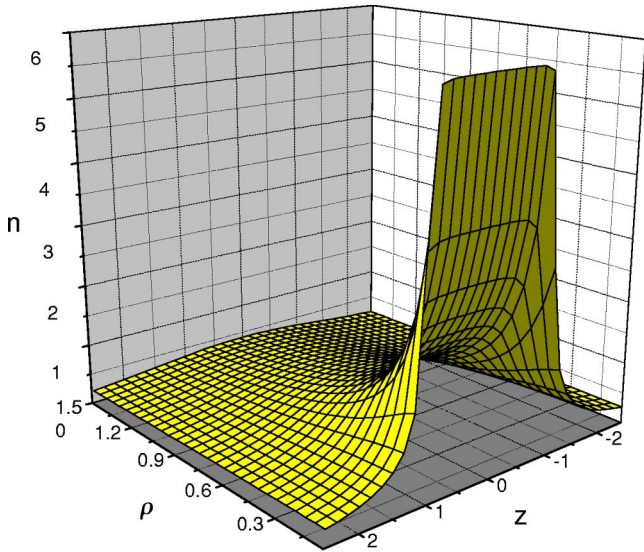


FIG. 3. The segment density distribution  $n(\rho, z)$  obtained from the linearized Euler-Lagrange equations; note that  $n(\rho, z)$  diverges when  $\rho \rightarrow 0$  and  $z \pm L/2 \leq 0$ .

which are characteristic, respectively, of cylindrical [cf. Eq. (23)] and spherical polymer brushes [4].

The field  $f_4(\rho, z)$  is most easily calculated with the help of functions  $\Phi(\alpha_1, \alpha_2)$ ,  $R(\alpha_1, \alpha_2)$ , and  $g(\alpha_1, \alpha_2)$ , defined in Eq. (31). Rewriting Eqs. (37) in the angle coordinates  $\alpha_1$  and  $\alpha_2$ , we find

$$\Phi(\alpha_1, \alpha_2) = \frac{\alpha_2 - \alpha_1}{2}, \quad R(\alpha_1, \alpha_2) = \cos\left(\frac{\alpha_2 + \alpha_1}{2}\right). \quad (42)$$

Note that, within the approximations made, the functions  $\Phi(\alpha_1, \alpha_2)$  and  $R(\alpha_1, \alpha_2)$  are analytic everywhere in the triangle  $\alpha_1 + \alpha_2 \leq \pi$ . The function  $g(\alpha_1, \alpha_2)$  is found as a unique (numerical) solution to Eqs. (33), (34) and (42). If  $N$  is the degree of polymerization of side chains in a bottle-brush molecule, the resulting field  $f_4(\rho, z)$  determines the shape of the molecule's surface via the relationship  $f_4(\rho, z) = N$ . In the special case of  $\alpha_1 = \alpha_2$ , the function  $g(\alpha_1, \alpha_2)$  admits the analytic representation,

$$g(\alpha_1) = \cot^{4/3} \alpha_1 \int_0^{\alpha_1} \sin^{1/3} x \cos^{-8/3} x dx. \quad (43)$$

Solving the equation

$$\frac{1}{2^{1/3}} R_g^{4/3} g(\arctan(R_g)) = N, \quad (44)$$

where  $g$  is given by Eq. (43), we obtain the linear size  $R_g$  of a central chain as a function of  $N$ . The resulting dependence  $R_g(N)$  reveals two different scaling regimes that are clearly shown in Fig. 4,

$$R_g \sim \begin{cases} N^{3/4}, & N \ll 1 \\ N^{3/5}, & N \gg 1. \end{cases} \quad (45)$$

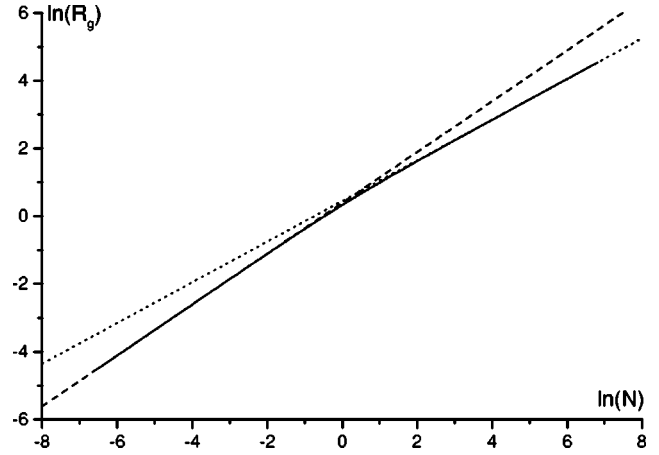


FIG. 4. Double logarithmic plot of the end-to-end distance  $R_g$  of a central chain as a function of the degree of polymerization  $N$  (solid line). The dashed line  $y = 0.75x + 0.39$  and the dotted line  $y = 0.6x + 0.45$  correspond, respectively, to the scaling limits of cylindrical and spherical polymer brushes.

These scaling relationships are identical to those that have been obtained individually for cylindrical [cf. Eq. (22)] and spherical polymer brushes [4]. Recall that the half length of the backbone is set everywhere to 1, so, in fact,  $N$  substitutes for the combination of quantities  $N(L/2)^{-4/3}$ . Hence, in the present notation, the values of  $N$  may be both small and large (see also discussion below).

Here we do not present the complete results of the numerical solution for  $g(\alpha_1, \alpha_2)$  and  $f_4(\rho, z)$ . According to these results, the shape of a bottle-brush molecule changes from a prolonged cylinder when  $N \ll 1$  to almost a sphere when  $N \gg 1$ . A similar change of shape is observed for a surface of constant density  $n(\rho, z) = n_0$ , when the value of parameter  $n_0$  is decreased. Examples of such surfaces are shown in Fig. 2 for three different values of  $n_0$  that correspond to  $R_g = 0.2, 1$ , and  $5$ . Let us stress again that, if the half length of the backbone does not equal 1, we must replace  $N$  with the combination of parameters  $N(L/2)^{-4/3}$ . The latter can be presented in the form of the ratio  $(L/L_c)^{-4/3}$ , where  $L_c \sim N^{3/4}$ . As we already know, the transverse size  $R_g$  of a cylindrical polymer brush obeys the same scaling as the parameter  $L_c$ , namely,  $R_g \sim N^{3/4}$ . Hence, this is the ratio  $L/R_g$  which governs the crossover between the cylindrical and the spherical conformations of a bottle-brush molecule.

## VI. SOME COMMENTS ON THE NONLINEAR EQUATIONS

In the preceding section, we succeeded in finding an approximate solution to the Euler-Lagrange equations which gave a satisfactory description of the examined crossover. To find this approximate solution, we made an assumption that the dominant trajectories of chains are everywhere perpendicular to a surface of constant density. Such an assumption is, obviously, valid for infinitely long cylindrical brushes, as well as for spherically symmetric polymer stars. In the case of a bottle-brush molecule, we expect the angle  $\Theta$  between the trajectories of grafted chains and any surface of constant

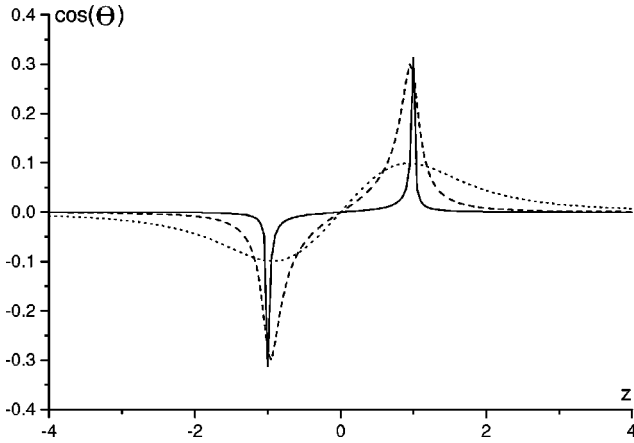


FIG. 5. Angle  $\Theta$  between the dominant trajectories of chains and a surface of constant density, as a function of  $z$ , and for three different values of  $\rho$ :  $\rho=0.01$  (solid line),  $0.1$  (dashed line), and  $1$  (dotted line).

density to be approximately  $90^\circ$  (1) in the immediate vicinity of the backbone *but* not very close to its ends, where the molecule's structure is similar to that of an infinitely long cylindrical brush and (2) anywhere far from the backbone, where the molecule's structure becomes spherically symmetric. To substantiate this quantitatively, we calculated  $\cos \Theta$ ,

$$\cos \Theta = \frac{\left( \frac{\partial n}{\partial \rho} \frac{\partial f_3}{\partial \rho} + \frac{\partial n}{\partial z} \frac{\partial f_3}{\partial z} \right)}{\sqrt{\left( \frac{\partial n}{\partial \rho} \right)^2 + \left( \frac{\partial n}{\partial z} \right)^2} \sqrt{\left( \frac{\partial f_3}{\partial \rho} \right)^2 + \left( \frac{\partial f_3}{\partial z} \right)^2}}, \quad (46)$$

using Eqs. (37) and the last of Eqs. (26). The results are presented in Fig. 5 for three different values of  $\rho$ , namely,  $\rho=0.01$ ,  $0.1$ , and  $1$ . We see that, when  $\rho \rightarrow 0$ , the value of  $\cos \Theta$  deviates from zero only in the immediate vicinity of the backbone ends. (Note that the maximum value of  $\cos \Theta$  is  $0.316$  which yields the minimum value of  $\Theta$  of approximately  $72^\circ$ .) When  $\rho$  is increased, the maximum value of  $\cos \Theta$  decreases, as the shape of a bottle-brush molecule becomes more spherical.

Thus, the linearized Euler-Lagrange equations need to be corrected only near the backbone, i.e., when  $\rho \ll 1$ . As shown in Fig. 1, the angle coordinates  $\alpha_1$  and  $\alpha_2$  become infinitely small if  $\rho \rightarrow 0$  and  $|z \pm L/2| \neq 0$ . When both  $\rho$  and  $|z - L/2|$  tend to zero, the value of  $\alpha_1$  remains finite, whereas  $\alpha_2 = 0$ , and determines the direction in which the upper end of the backbone is approached:  $\alpha_1 \in [0, \pi]$ . Similarly, for the lower end of the backbone we have  $\alpha_1 = 0$  and  $\alpha_2 \in [0, \pi]$ . We see that, for each point in the vicinity of the backbone, either  $\alpha_1$  or  $\alpha_2$  is very small. Equations (32) and (33) can be significantly simplified if we put one of the angle coordinates to zero. For instance, for  $\alpha_2 = 0$  we have

$$\frac{\partial \Phi}{\partial \alpha_1} = \frac{\sin \Phi}{\sin \alpha_1} \frac{\cos(\Phi + \alpha_1)}{[2 + \cos 2(\Phi + \alpha_1)]},$$

$$\frac{\partial \ln R}{\partial \alpha_1} = \tan(\Phi + \alpha_1) \frac{\partial \Phi}{\partial \alpha_1},$$

$$\frac{4}{3} g \cos \Phi + \sin \alpha_1 \frac{\partial g}{\partial \alpha_1} \cos(\Phi + \alpha_1) - R^{-1/3} = 0. \quad (47)$$

In order to satisfy Eqs. (47) and the boundary conditions of Eq. (34), functions  $\Phi(\alpha_1, 0)$ ,  $R(\alpha_1, 0)$ , and  $g(\alpha_1, 0)$  must have the following series expansions:

$$\Phi = C \alpha_1^{1/3} + O(\alpha_1^{5/3}),$$

$$R = 1 + \frac{1}{2} C^2 \alpha_1^{2/3} + O(\alpha_1^{4/3}),$$

$$g = \frac{3}{4} + \frac{1}{6} C^2 \alpha_1^{2/3} + O(\alpha_1^{4/3}). \quad (48)$$

In these expansions, the value of constant  $C$ , namely  $C = -2^{-1/3}$ , is found from the condition that numerical integration of the first of Eqs. (47) yields [cf. Eq. (42)]

$$\Phi(\alpha_1 \rightarrow \pi) = -\alpha_1/2. \quad (49)$$

The functions  $\Phi(\alpha_1, 0)$ ,  $R(\alpha_1, 0)$ , and  $g(\alpha_1, 0)$ , obtained by numerical integration of Eqs. (47) under the boundary conditions of Eqs. (48), are plotted in Fig. 6, where they are also compared to the approximate results of the preceding section [11]. We see a significant quantitative discrepancy between the two sets of curves [which is not as striking for the curves  $g(\alpha_1, 0)$ , compared in Fig. 6(c), since they both were obtained by solving the same Eq. (33)]. Apart from the quantitative differences, the exact solution  $R(\alpha_1, 0)$  shows a qualitatively new feature, namely, its maximum is positioned at  $\alpha_1 \neq 0$  [see Fig. 6(b)]. Such a positioning of the maximum is responsible for the appearance of the "ears" around the ends of the backbone in the segment density distribution  $n(\rho, z)$ . This is illustrated in Fig. 7 which presents a sketch of the three-dimensional surface  $n(\rho, z)$  (cf. Fig. 3). Below, we explain how this surface was obtained.

Equations (48) can be generalized to the case of two variables so as to satisfy Eqs. (32) and (33). We find the following expansions for  $\Phi(\alpha_1, \alpha_2)$  and  $R(\alpha_1, \alpha_2)$ :

$$\Phi = \frac{2^{2/3}}{2} \alpha_0^{1/3} f \left( \frac{\alpha_2 - \alpha_1}{\alpha_1 + \alpha_2} \right) + O(\alpha_0^{5/3}),$$

$$R = 1 + \frac{2^{1/3}}{4} \alpha_0^{2/3} f^2 \left( \frac{\alpha_2 - \alpha_1}{\alpha_1 + \alpha_2} \right) + O(\alpha_0^{4/3}), \quad (50)$$

where  $\alpha_0 = \alpha_1 + \alpha_2$ , and  $f(x)$  is some odd function of  $x$  such that  $f(1) = 1$ . The specific form of function  $f$  should be determined by the condition that numerical solution of Eqs. (32), under the boundary conditions of Eqs. (50), agrees with the results of Eq. (42) when  $\alpha_0 \rightarrow \pi$  and  $\alpha_{1,2} \neq 0$ . However, for technical reasons, we were not able to find such a solution and, hence, to determine  $f$ . Our algorithm for the self-consistent numerical integration of Eqs. (32) is described in Appendix B. It seems to be very sensitive to the boundary

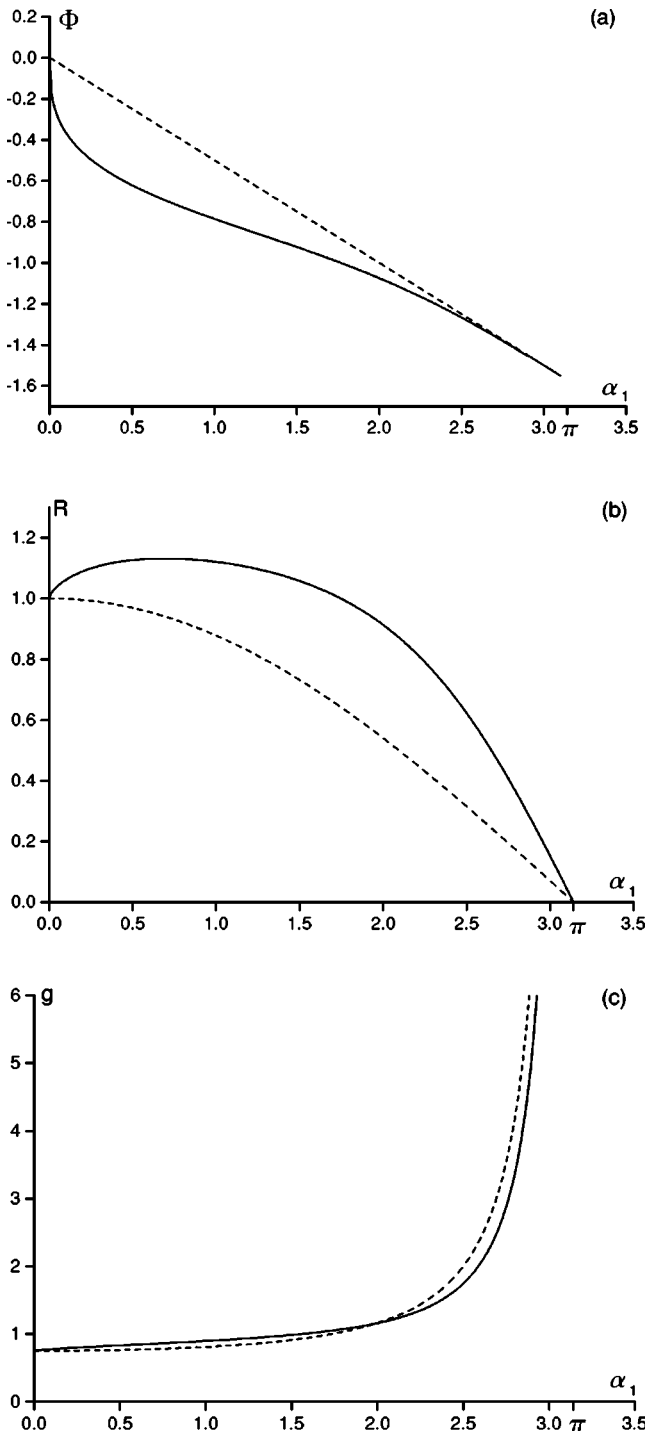


FIG. 6. Functions (a)  $\Phi(\alpha_1,0)$ , (b)  $R(\alpha_1,0)$ , and (c)  $g(\alpha_1,0)$  found as a solution to the exact Euler-Lagrange equations (solid lines). The dashed lines stand for the approximate results given by Eqs. (33) and (42).

conditions and, since we do not know *a priori*, it inevitably breaks down at some point (generally, at  $\alpha_0 \approx 2.1-2.5$ ), as we move away from  $0 < \alpha_0 \leq 1$  to larger values of  $\alpha_0$ . We note that we used the same algorithm in order to find  $g(\alpha_1, \alpha_2)$  in the preceding section, and we did not encounter any problems in building the full numerical solution to Eq. (33), where  $\Phi$  and  $R$  were given by Eq. (42).

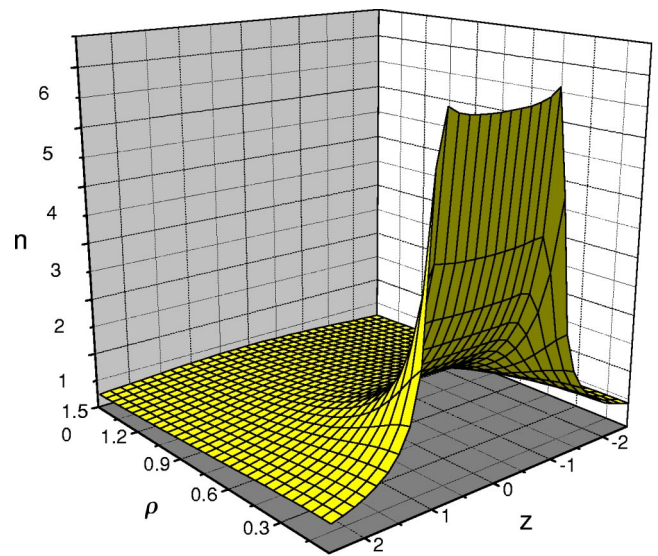


FIG. 7. The segment density distribution  $n(\rho, z)$  found from the nonlinear Euler-Lagrange equations. Note the new effect of “ears” around the ends of the backbone, which is missing in Fig. 3. It appears due to the maximum in the exact dependence  $R(\alpha_1,0)$ , shown in Fig. 6(b).

In order to obtain a qualitatively valid solution to Eqs. (32), we may use the following approximate form of  $\Phi$ :

$$\Phi^{app}(\alpha_1, \alpha_2) = \frac{\alpha_2 - \alpha_1}{\alpha_1 + \alpha_2} \Phi(\alpha_0, 0), \quad (51)$$

and simply calculate  $R^{app}(\alpha_1, \alpha_2)$  from the second of Eqs. (32). It is straightforward to see that  $\Phi^{app}$  satisfies the first of Eqs. (50) with  $f(x) = x$ , as well as provides the correct asymptotic behavior when  $\alpha_0 \rightarrow \pi$  [cf. Eq. (42)]. Besides, for all those  $\alpha_0$  — for which we were able to build a self-consistent solution to Eqs. (32), under the condition that  $f(x) = x$  — the functions  $\Phi$  and  $R$ , resulting from such a solution, were qualitatively very similar to  $\Phi^{app}$  and  $R^{app}$ . Thus, the segment density distribution  $n(\rho, z)$  shown in Fig. 7 has been obtained from  $R^{app}$  and the third of Eqs. (32). Let us stress that the effect of “ears” is independent of any specific form of  $f$  or  $\Phi^{app}$ , and is solely due to the maximum in the exact dependence  $R(\alpha_1, 0)$  [see Fig. 6(b)]. However, the correct specific form of  $f$  is necessary to fulfill the condition of spherical symmetry for  $R(\alpha_1, \alpha_2)$  when  $\alpha_0 \rightarrow \pi$  and  $\alpha_{1,2} \neq 0$ , which is not satisfied by  $R^{app}$ .

Let us now comment on the following peculiarities of the cylindrical polymer brushes of finite length. We know that, in a polymer brush with  $L \rightarrow \infty$ , the trajectories of all chains are perpendicular to the line of the backbone. When  $L$  is finite, the angle between the trajectory of a given chain and the axis  $z$  may change depending on the chain’s grafting point. Thus, in the central part of a polymer brush, the chains remain perpendicular to the axis  $z$  ( $\alpha_1 \approx 0$ ), while the chains grafted near the backbone ends are almost parallel to it ( $\alpha_1 \approx \pi$ ). We can study the properties of the mentioned chains by taking

the relevant limits in the functions  $R(\alpha_1, 0)$  and  $g(\alpha_1, 0)$ . In the limit  $\alpha_1 \rightarrow 0$ , we have  $R(\alpha_1, 0) = 1$  and  $g(\alpha_1, 0) = 3/4$  which result in

$$n(\rho, z) = \frac{1}{2^{1/3}} \rho^{-2/3}, \quad f_4(\rho, z) = \frac{3}{4} \frac{1}{2^{1/3}} \rho^{4/3}. \quad (52)$$

Note that the exponents in Eqs. (52) correspond to the cylindrical symmetry, which is rather obvious since Eqs. (47) are only valid near the backbone. In the opposite limit  $\alpha_1 \rightarrow \pi$ , the numerical integration yields  $R(\alpha_1, 0) = C(\pi - \alpha_1)$  and  $g(\alpha_1, 0) = 3/4 C^{-1/3} (\pi - \alpha_1)^{-4/3}$ , where  $C \approx 1.086$ . This leads to

$$n(\rho, z) = \frac{C^{2/3}}{2^{1/3}} (z-1)^{-2/3}, \quad f_4(\rho, z) = \frac{3}{4} \frac{C^{-1/3}}{2^{1/3}} (z-1)^{4/3}. \quad (53)$$

In the limits considered,  $\rho$  and  $z-1$  stand for the same quantity, namely the distance to the backbone  $r_t$  calculated along the chain. Therefore, both Eqs. (52) and (53) can be rewritten in the form

$$n(r_t) \approx \frac{1}{2^{1/3}} r_t^{-2/3}, \quad f_4(r_t) \approx \frac{3}{4} \frac{1}{2^{1/3}} r_t^{4/3}. \quad (54)$$

The above scaling relationships have been obtained for the chains grafted either in the center of a polymer brush or near the ends of its backbone. We assume, however, that Eqs. (54) are also valid for all grafted chains. Then any surface  $f_4(r_t) = t$  which consists of all segments  $t$  can also be considered as a surface of constant density  $n(r_t) = n_0$ . Clearly, if  $r_t$  is such that  $t = N$ , the surface of constant density is identical to the external surface of a polymer brush. According to Eqs. (54), as well as computer simulations [12], the polymer chains in a bottle-brush molecule are all equally extended. This allows us to model the molecule's surface as a prolate ellipsoid of the form

$$\frac{\rho^2}{R_g^2} + \frac{z^2}{(1+R_g)^2} = 1, \quad (55)$$

where  $R_g$  denotes the linear size of a central chain (recall  $L/2 \equiv 1$ ). Let us recall that Eqs. (54) were obtained in the immediate vicinity of the backbone. However, the conclusions drawn from them are automatically valid at large distances from the backbone, where a bottle-brush molecule becomes spherically symmetric. This leads us to believe that the results of the preceding paragraph, including Eq. (55), apply to any length scales inside a bottle-brush molecule.

## VII. CONCLUSION

We have presented a quantitative study of a single bottle-brush molecule, which consists of a stiff backbone of length  $L$  grafted densely with flexible polymer chains. Since the grafted chains are strongly stretched in the presence of excluded volume interactions, we consider only their dominant

trajectories. Such dominant trajectories are found as a solution to the nonlinear Euler-Lagrange equations, resulting from minimization of the free energy functional. If we assume that the trajectories of chains are everywhere perpendicular to a surface of constant (segment) density, the Euler-Lagrange equations can be linearized and solved analytically. This assumption is valid everywhere except for the immediate vicinity of the backbone, where we have found a numerical solution to the full nonlinear equations.

We have shown that the dominant trajectories of chains are curved towards the ends of the backbone. Due to the bending of chains, the segment density in the center of a polymer brush is only 5.5% lower than that calculated near the backbone ends [cf. the first of Eqs. (52) and (53)]. Also, the stretching of the side chains was shown to be independent of where exactly these chains are grafted. We believe, therefore, that all local properties of bottle-brush polymers are fairly homogeneous. As a result of this homogeneity, any surface created by all segments with number  $t$  is also a surface of constant density. Apparently, if  $N$  is the degree of polymerization of side chains and  $t = N$ , the surface of constant density is identical to the external surface of a polymer brush. The latter is found to have the shape of a prolate ellipsoid, which seems to be in agreement with experimental data [13–15].

Furthermore, we have discovered the elements of two different symmetries in the structure of a single bottle-brush molecule. We have shown that the trajectories of all chains start perpendicular to the line of the backbone, which is distinctive of infinitely long *cylindrical* brushes. As the distance to the backbone increases, the chains begin to deviate from their initial direction and the cylindrical structure is destroyed. If the distance to the backbone is very large, the trajectory of each chain represents a straight line whose slope is dependent on where the given chain is joined to the backbone. There is an equal number of straight lines heading in each direction, which corresponds to the *spherically* symmetric structure of a polymer star. We have determined the cylindrical and spherical limits for all local characteristics of bottle-brush molecules. The crossover between these limits occurs at the distances to the backbone comparable with its size  $L$ , or for the segment numbers  $t \sim L^{4/3}$ . We note that the resulting crossover regions are rather broad and, therefore, some knowledge of the full crossover functions is required.

## ACKNOWLEDGMENTS

I am grateful to Professor Jean-Pierre Hansen for his help in preparation of this manuscript. I also acknowledge financial support from St. John's College, University of Cambridge.

## APPENDIX A: REPRESENTING THE EULER-LAGRANGE EQUATIONS IN CYLINDRICAL COORDINATES

In this appendix, we present the derivation of Eqs. (26) of the main text. We start with the expression for the total segment density  $n$ , given by Eq. (18), and rewrite it using Eqs. (13). We find

$$\begin{aligned}
 n &= \frac{1}{2} \left[ \left( \frac{\partial f_1}{\partial t} \right)^2 + \left( \frac{\partial f_2}{\partial t} \right)^2 \right] = \frac{1}{2} D_{-1}^2 \left[ \left( \frac{\partial f_3}{\partial z} \right)^2 + \left( \frac{\partial f_3}{\partial \rho} \right)^2 \right] \\
 &= \frac{1}{2} f_1^2 D_{-1}^2 \left[ \frac{1}{\rho^2} \left( \frac{\partial f_3}{\partial z} \right)^2 + \frac{1}{\rho^2} \left( \frac{\partial f_3}{\partial \rho} \right)^2 \right] = \frac{1}{2n^2} (x_1^2 + x_2^2),
 \end{aligned}
 \tag{A1}$$

and thus we have obtained the third of Eqs. (26). Let us now derive the first of these equations. Differentiating Eq. (18) with respect to  $z_0$  yields

$$\frac{\partial}{\partial z_0} n(z_0, t) = \frac{\partial f_1}{\partial t} \frac{\partial^2 f_1}{\partial t \partial z_0} + \frac{\partial f_2}{\partial t} \frac{\partial^2 f_2}{\partial t \partial z_0}, \tag{A2}$$

and, independently from Eq. (A2), we find using the rules of partial differentiation and Eqs. (15),

$$\begin{aligned}
 \frac{\partial}{\partial z_0} n(z_0, t) &= \frac{\partial f_1}{\partial z_0} \frac{\partial}{\partial \rho} n(\rho, z) + \frac{\partial f_2}{\partial z_0} \frac{\partial}{\partial z} n(\rho, z) \\
 &= \frac{\partial f_1}{\partial z_0} \frac{\partial^2 f_1}{\partial t^2} + \frac{\partial f_2}{\partial z_0} \frac{\partial^2 f_2}{\partial t^2}.
 \end{aligned}
 \tag{A3}$$

Subtracting Eq. (A2) from Eq. (A3) and replacing the first-order derivatives as prescribed by Eqs. (13), we get

$$- \left( \frac{\partial^2 f_1}{\partial t^2} \frac{\partial f_4}{\partial z} + \frac{\partial^2 f_1}{\partial t \partial z_0} \frac{\partial f_3}{\partial z} \right) + \left( \frac{\partial^2 f_2}{\partial t^2} \frac{\partial f_4}{\partial \rho} + \frac{\partial^2 f_2}{\partial t \partial z_0} \frac{\partial f_3}{\partial \rho} \right) = 0, \tag{A4}$$

which, in turn, folds to give a fairly simple relationship,

$$- \frac{\partial}{\partial z} \left( \frac{\partial f_1}{\partial t} \right) + \frac{\partial}{\partial \rho} \left( \frac{\partial f_2}{\partial t} \right) = 0. \tag{A5}$$

Finally, combining Eqs. (A5) and (13) yields

$$\frac{\partial}{\partial z} \left( D_{-1} \frac{\partial f_3}{\partial z} \right) + \frac{\partial}{\partial \rho} \left( D_{-1} \frac{\partial f_3}{\partial \rho} \right) = 0. \tag{A6}$$

It is straightforward to see that Eq. (A6) is equivalent to the first of Eqs. (26). As to the second of Eqs. (26), its origin is explained in the main text.

### APPENDIX B: NUMERICAL SOLUTION OF THE NONLINEAR EQUATIONS

In this appendix, we present an algorithm to solve a first-order partial differential equation depending on  $\alpha_1$  and  $\alpha_2$ , or a system of such equations. For the purpose of numerical integration, we employ the two-dimensional grid shown in Fig. 8. The number of grid points  $M$  is the same both for  $\alpha_1$  and  $\alpha_2$ , and the increment  $\delta = \pi/(M-1)$ . Each point on the grid is defined by two indices  $i$  and  $n$ , where  $i$  counts the lines of constant  $\alpha_1$ :  $\alpha_1(i, n) = \delta(i-1) \forall n$ , and  $n$  counts the lines of constant  $\alpha_0 = \alpha_1 + \alpha_2$ :  $\alpha_0(i, n) = \delta(n-1) \forall i$ . In order to build a complete numerical solution, we move step by step, from diagonal  $n-1$  to diagonal  $n$ , starting from some  $n=n_0$ . As an example, let us consider the first two of

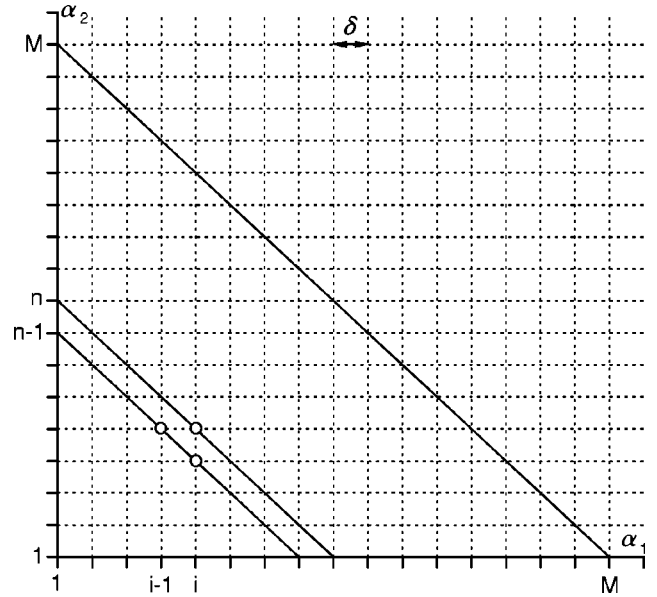


FIG. 8. Two-dimensional grid used for the numerical integration of the nonlinear Euler-Lagrange equations.

Eqs. (32). We can rewrite these equations in terms of finite differences, which involves three grid points, as shown in Fig. 8. We have

$$\begin{aligned}
 &K_3[\bar{R}(i, n) - \bar{R}(i-1, n-1)] + K_4[\bar{R}(i, n) - \bar{R}(i, n-1)] \\
 &\quad + 3K_1[\Phi(i, n) - \Phi(i-1, n-1)] \\
 &\quad + 3K_2[\Phi(i, n) - \Phi(i, n-1)] - \delta \sin[\Phi(i, n)] = 0, \\
 &K_1[\bar{R}(i, n) - \bar{R}(i-1, n-1)] + K_2[\bar{R}(i, n) - \bar{R}(i, n-1)] \\
 &\quad - K_3[\Phi(i, n) - \Phi(i-1, n-1)] \\
 &\quad - K_4[\Phi(i, n) - \Phi(i, n-1)] = 0,
 \end{aligned}
 \tag{B1}$$

where

$$\begin{aligned}
 K_1 &= \sin[\alpha_1(i, n)] \cos[\Phi(i, n) + \alpha_1(i, n)], \\
 K_2 &= \sin[\alpha_2(i, n)] \cos[\Phi(i, n) - \alpha_2(i, n)], \\
 K_3 &= \sin[\alpha_1(i, n)] \sin[\Phi(i, n) + \alpha_1(i, n)], \\
 K_4 &= \sin[\alpha_2(i, n)] \sin[\Phi(i, n) - \alpha_2(i, n)].
 \end{aligned}
 \tag{B2}$$

Equations (B1) can be solved with respect to  $\Phi(i, n)$  and  $\bar{R}(i, n)$ . Thus, if the values of  $\Phi$  and  $\bar{R}$  are known on diagonal  $n-1$ , they can also be determined at each point on diagonal  $n$ . As initial conditions, we need to know the corresponding values at  $n=n_0$ .

Unfortunately, we were not able to build a complete solution to Eqs. (32), using the algorithm described above. We tend to think that this algorithm is very sensitive to the initial values of  $\Phi$  and  $\bar{R}$  which, in our case, we do not know *a priori*. Instead, we try to guess these initial values so as to

retrieve spherical symmetry when  $\alpha_0 \rightarrow \pi$  and  $\alpha_{1,2} \neq 0$ . Our guesses are, obviously, not close enough to the true answer, and this gives rise to growing fluctuations at some  $n < M$ . However, we were able to successfully implement this

algorithm in order to find a solution to Eq. (33), where  $\Phi$  and  $R$  were given by Eq. (42). In this case, we started with  $n_0 = 1$  and  $g(1,1) = 3/4$ , and did not encounter any problems in moving all the way up to  $n = M$ .

- 
- [1] T.M. Birshtein, O.V. Borisov, E.B. Zhulina, A.R. Khokhlov, and T.A. Yurasova, *Polym. Sci. U.S.S.R.* **29**, 1293 (1987).
- [2] R.S. Ball, J.F. Marco, S.T. Milner, and T.A. Witten, *Macromolecules* **24**, 693 (1991).
- [3] G.H. Fredrickson, *Macromolecules* **26**, 2825 (1993).
- [4] H. Li and T.A. Witten, *Macromolecules* **27**, 449 (1994).
- [5] K. Shiokawa, *Polym. J. (Tokyo, Jpn.)* **27**, 871 (1995).
- [6] M.A. Carignano and I. Szleifer, *J. Chem. Phys.* **102**, 8662 (1995).
- [7] A. Subbotin, M. Saariaho, O. Ikkala, and G. ten Brinke, *Macromolecules* **33**, 3447 (2000).
- [8] A. Subbotin, M. Saariaho, R. Stepanyan, O. Ikkala, and G. ten Brinke, *Macromolecules* **33**, 6168 (2000).
- [9] N. A. Denesyuk *Phys. Rev. E* **67**, 051803 (2003).
- [10] S. Alexander, *J. Phys. (Paris)* **38**, 977 (1977).
- [11] For the purpose of numerical integration, we cannot use the boundary conditions of Eq. (34), since all three functions  $\Phi(\alpha_1 0)$ ,  $R(\alpha_1 0)$ , and  $g(\alpha_1 0)$  are nonanalytic at  $\alpha_1 = 0$ . Instead, we start integrating from some nonzero value of  $\alpha_1 \ll 1$ , employing the boundary conditions that result from Eqs. (48).
- [12] K. Shiokawa, K. Itoh, and N. Nemoto, *J. Chem. Phys.* **111**, 8165 (1999).
- [13] M. Wintermantel, M. Schmidt, Y. Tsukahara, K. Kajiwara, and S. Kohjiya, *Macromol. Rapid Commun.* **15**, 279 (1994).
- [14] N. Nemoto, M. Nagai, A. Koike, and S. Okada, *Macromolecules* **28**, 3854 (1995).
- [15] M. Wintermantel, M. Gerle, K. Fischer, M. Schmidt, I. Wataoka, H. Urakawa, K. Kajiwara, and Y. Tsukahara, *Macromolecules* **29**, 978 (1996).